

Solvation-mediated adsorption mechanism of solvated lithium ions
at charged solid-liquid interface for electrochemical energy storage:
Atomic scale investigation and insights.

Muhammad Hamza^a, Bing-Ang Mei^{a *}, Ridong Liao^a, Huihua Feng^a, Zhengxing Zuo^a, Zia ul
Rehman Tahir^b, Rui Xiong^a

^a School of Mechanical Engineering, Beijing Institute of Technology, Beijing 100081, China

^b Faculty of Mechanical Engineering, University of Engineering and Technology, Lahore,
Pakistan

*Corresponding author:

Tel: +86-10-68913041

E-mail: meiba@bit.edu.cn

February 8, 2025

Supplementary material

Bonded and non-bonded interactions for Class II force field

The potential energy of intermolecular interaction E_{inter} was given by the superposition of LJ 9-6 and coulombic interactions, expressed as

$$E(r)_{inter} = \sum_{VW} \epsilon_{ij} \left[2 \left(\frac{\sigma_{ij}}{r_{ij}} \right)^9 - 3 \left(\frac{\sigma_{ij}}{r_{ij}} \right)^6 \right] + \sum_{Coulomb} \frac{q_i q_j}{r_{ij}} \quad (S1)$$

where ϵ and σ are the so called LJ parameter representing well depth and Van der Waals radius, respectively. The subscripts i and j represent the two interacting atoms. On the other hand, the potential energy of intramolecular interaction E_{intra} obtained from class II force field for molecules can be expressed as [1–8]

$$\begin{aligned} E(r)_{intra} = & \sum_b \left[{}^2K_b (b - b_0)^2 + {}^3K_b (b - b_0)^3 + {}^4K_b (b - b_0)^4 \right] \dots \\ & + \sum_\theta \left[{}^2K_\theta (\theta - \theta_0)^2 + {}^3K_\theta (\theta - \theta_0)^3 + {}^4K_\theta (\theta - \theta_0)^4 \right] \dots \\ & + \sum_\phi \left[{}^1K_\phi (1 - \cos \phi) + {}^2K_\phi (1 - \cos 2\phi) + {}^3K_\phi (1 - \cos 3\phi) \right] \dots \\ & + \sum_b \sum_{b'} K_{bb'} (b - b_0) (b' - b'_0) \dots \\ & + \sum_\theta \sum_{\theta'} K_{\theta\theta'} (\theta - \theta_0) (\theta' - \theta'_0) \dots \\ & + \sum_b \sum_\theta K_{b\theta} (b - b_0) (\theta - \theta_0) \dots \\ & + \sum_\phi \sum_b (b - b_0) \left[{}^1K_{\phi b} \cos \phi + {}^2K_{\phi b} \cos 2\phi + {}^3K_{\phi b} \cos 3\phi \right] \dots \\ & + \sum_\phi \sum_{b'} (b' - b'_0) \left[{}^1K_{\phi b'} \cos \phi + {}^2K_{\phi b'} \cos 2\phi + {}^3K_{\phi b'} \cos 3\phi \right] \dots \\ & + \sum_\phi \sum_\theta (\theta - \theta_0) \left[{}^1K_{\phi\theta} \cos \phi + {}^2K_{\phi\theta} \cos 2\phi + {}^3K_{\phi\theta} \cos 3\phi \right] \dots \\ & + \sum_\phi \sum_\theta \sum_{\theta'} K_{\phi\theta\theta'} (\theta - \theta_0) (\theta' - \theta'_0) \cos \phi \end{aligned} \quad (S2)$$

where K is the force constant, b , θ and ϕ represent the bond, angle and torsion between different bonded atoms while b' , θ' and ϕ' represent the neighboring bond, angle and torsion, respectively. Note that the superscript numbers on left side of K differentiate different force constant coefficients associated with various terms. In order to have an indepth view of these coefficients and what they signify, the reader is advised to go through these references [1–8]

Error analysis and background calculations for physical properties

Figure S1 shows the fitted mean square displacement (MSD) of (a) lithium and (b) PF₆ ions for different salt concentrations. Linear regression was performed to obtain the fitted MSD. However, the MSD run for the full simulation does not correspond to the diffusive regime where the simulation can be treated as the long times simulation necessary for calculation of diffusion coefficient using Einstein relation mentioned in the manuscript [9]. Usually, in order to identify the diffusive regime, the following exponential expression is used

$$\zeta = \frac{\ln(MSD) - \ln(m)}{\ln(t)} \quad (S3)$$

where m is the slope, \ln is the natural log and ζ is the exponent that needs to be evaluated to identify the diffusive regime for accurate diffusion coefficient calculation of ions. The value of the exponent should be one for the diffusive regime and to ensure that the simulation have reached the long time limit for the Einstein. Figure S2 shows the exponent ζ as a function of simulation time identifying the sub-diffusive and diffusive regimes for lithium ions in (a) 0.5 M, (b) 1.0 M, (c) 1.5 M and (d) 2.0 M salt concentrations. It shows that the long time limit has been reached and only the diffusive regime was used for the evaluation of diffusion coefficient reported in the manuscript. Similarly, Figure S3 shows the exponent ζ as a function of simulation time identifying the sub-diffusive and diffusive regimes for PF₆ ions in (a) 0.5 M, (b) 1.0 M, (c) 1.5 M and (d) 2.0 M salt concentrations. These figures for PF₆ also showed that the simulations have reached the diffusive regions for accurate calculation of diffusion coefficient for PF₆ ions. Furthermore, Figure S4 shows the viscosity the bulk electrolytes as a function of simulation time for (a) 0.5 M, (b) 1.0 M, (c) 1.5 M and (d) 2.0 M salt concentrations. The figures shows that the simulation was long enough for the values of viscosity to stabilize and reach an almost constant values. Additionally, Figure S5 shows the evaluated Green-Kubo expression for various pressure components. It shows that the average value of pressure correlation $\langle J(t) \cdot J(0) \rangle$ oscillatory decayed to zero with the increase in time. This validates the accuracy of the viscosity calculated by Green-Kubo expressions.

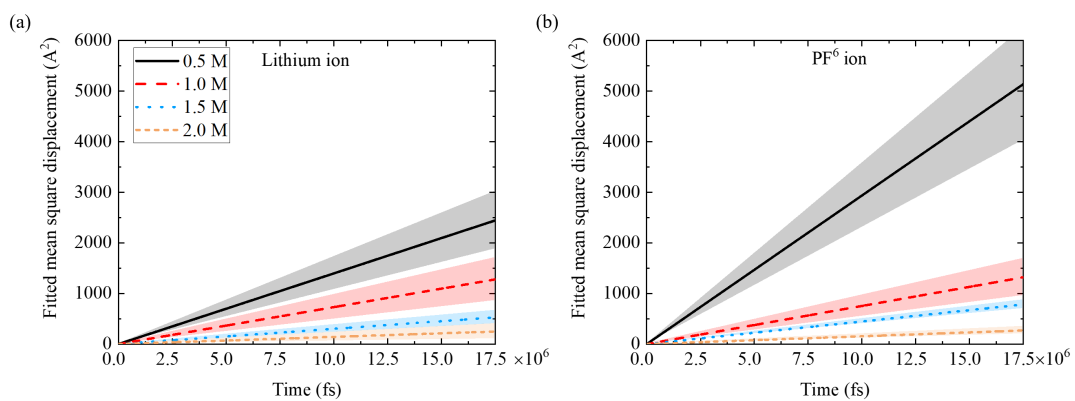


Figure S1: Fitted mean square displacement of (a) lithium and (b) PF_6 ions for different salt concentrations. The shaded region around the curve is the mean error of independent MD simulations relative to the mean.

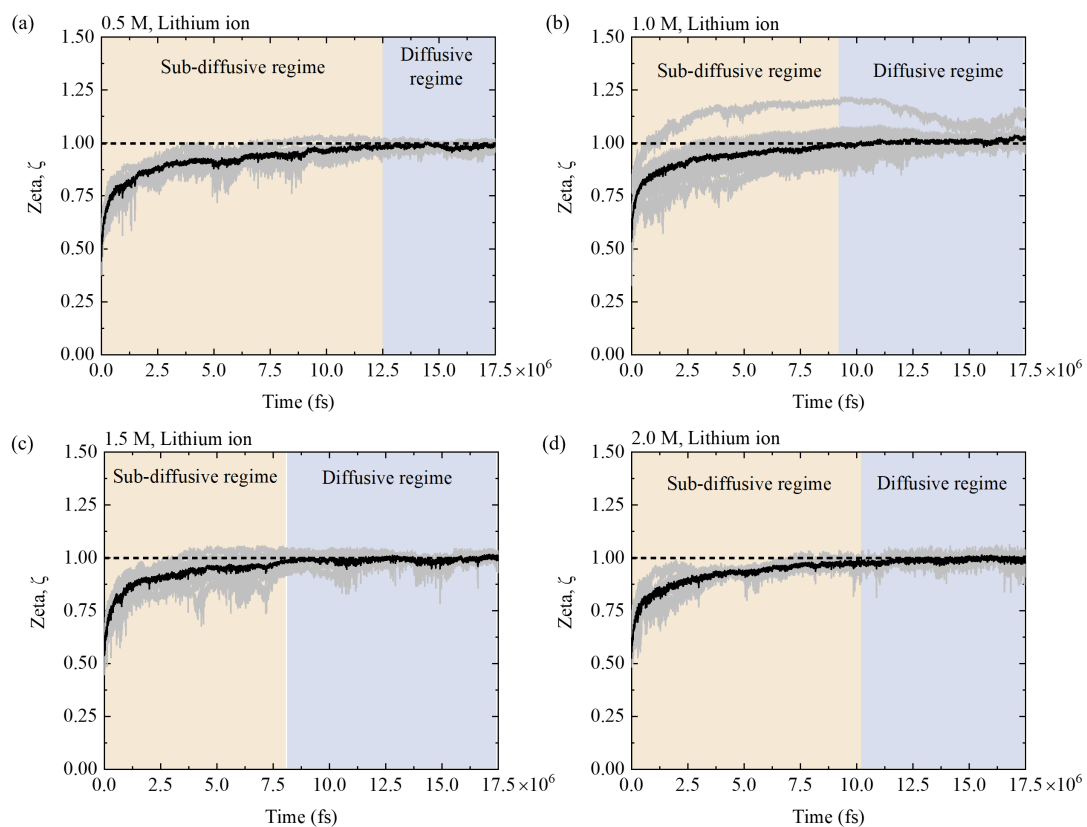


Figure S2: Exponent ζ as a function of simulation time identifying the sub-diffusive and diffusive regimes for lithium ions in (a) 0.5 M, (b) 1.0 M, (c) 1.5 M and (d) 2.0 M salt concentrations. The grey curves around the black (mean) curve represent the independent MD simulations.

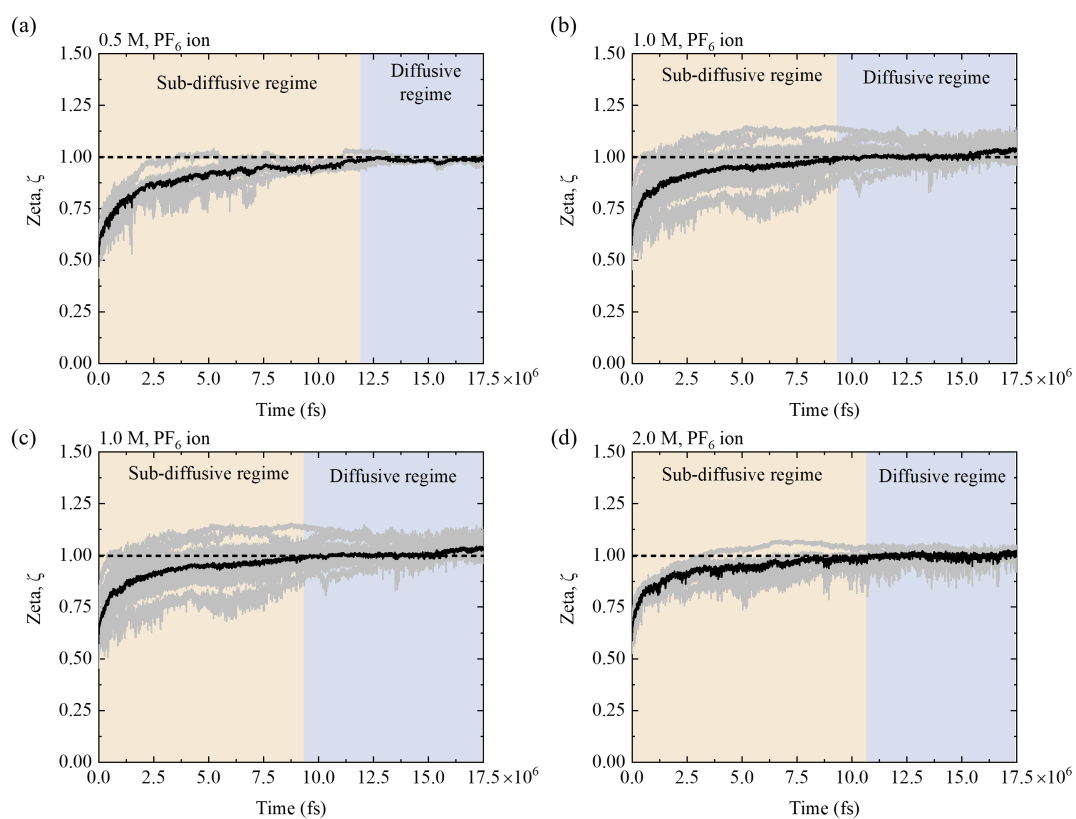


Figure S3: Exponent ζ as a function of simulation time identifying the sub-diffusive and diffusive regimes for PF_6 ions in (a) 0.5 M, (b) 1.0 M, (c) 1.5 M and (d) 2.0 M salt concentrations. The grey curves around the black (mean) curve represent the independent MD simulations.

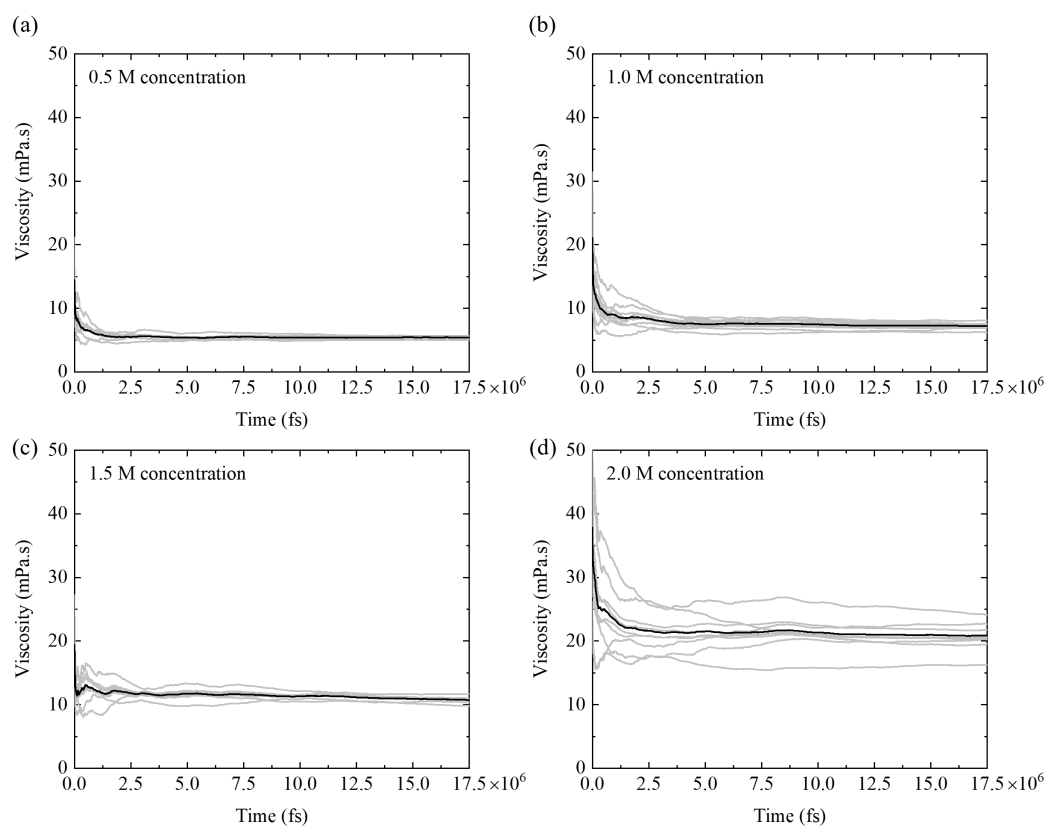


Figure S4: Viscosity the bulk electrolytes as a function of simulation time for (a) 0.5 M, (b) 1.0 M, (c) 1.5 M and (d) 2.0 M salt concentrations. The grey curves around the black (mean) curve represent the independent MD simulations.

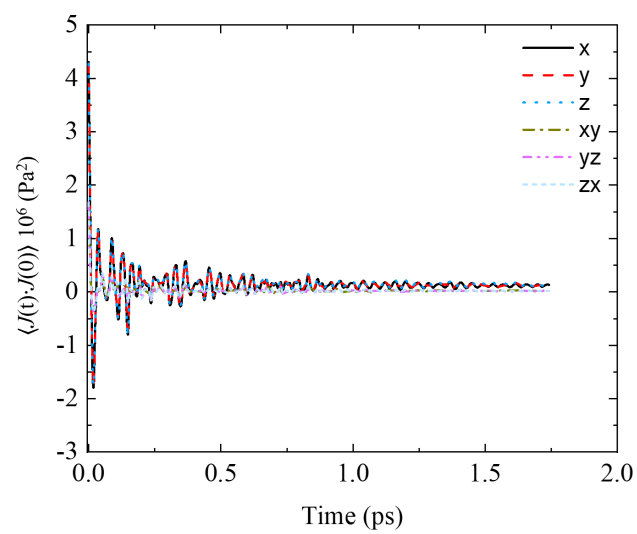


Figure S5: Temporal variation of Green-Kubo expression for various components of pressure.

Radial distribution function and coordination number analysis

Figure S6 shows the radial distribution function (RDF) and coordination number (CN) of (a)(b) Li-Li, (c)(d) Li-P and (e)(f) Li-F atoms in the electrolyte solution with increasing LiPF_6 concentration in PC. Li-Li RDF shows sharp peak which increased with increasing salt concentration followed by broad peaks. CN shows that it is not until 6-8 Å that the first lithium ion is located. This indicated weak solvation of lithium ion with other lithium ions. Similar trend was observed for Li-P and Li-F with increasing salt concentration. This kind of increasing trend of first sharp peak followed by broad peak with increasing salt concentration has also been reported in previous investigations [10].

Figure S7 shows the radial distribution function and coordination number of (a)(b) P-P, (c)(d) F-F and (e)(f) P-F atoms in the electrolyte solution with increasing LiPF_6 concentration in PC. P-P RDF shows two small peaks at 5 and 8 Å. CN number also reached unity approximately at this radial distance. This distance between P-P is expected as phosphorus atom of PF_6 is surrounded by six fluorine atoms. Increasing salt concentration does shows a slightly higher coordination number caused by the increase ions in the solution. F-F and P-F RDF showed two and one very sharp peaks for RDF, respectively. The CN were four and five for the two peaks of F-F and six for P-F peaks. These sharp peaks correspond to the other atoms within the same ions. These sharp peaks decrease in magnitude of RDF with increasing salt concentration as RDF is inversely proportional to the density of the non-central atoms when calculating RDF. These sharp peaks were followed by broad peaks which corresponded to atoms in other ions.

Figure S8 shows radial distribution function and coordination number of (a)(b) Li-C3, (c)(d) Li-C1 and (e)(f) Li-C2 atoms in the electrolyte solution with increasing LiPF_6 concentration in PC. The figures shows one distinct peak which remained unchanged with increasing salt concentration. CN also showed plateau corresponding to the RDF peak. Similarly, S9 shows radial distribution function and coordination number of (a)(b) Li-O, (c)(d) Li-Cc and (e)(f) Li-Oc (g)(h) Li-H atoms in the electrolyte solution with increasing LiPF_6 concentration in PC. These figure also showed distinct peak for RDF and CN which remained nearly constant except the peaks for Li-Oc and Li-Cc decreased with increasing salt concentration. The distinct peak can be attributed to the solvation of lithium ion with four PC molecules in the first solvation shell and 2-3 PC molecules in the second solvation shell. This RDF peak was sharpest for Li-Oc because lithium ion was directly attached to PC through Oc. The reason for this is discussed in detail in the manuscript. Finally, Figure S10 shows the radial distribution function and coordination number of (a)(b) Li-PC and (c)(d) PC-PC

atoms in the electrolyte solution with increasing LiPF_6 concentration in PC. Note that Li-PC and PC-PC corresponds to the centre-of-mass based RDF and CN. The figures show distinct peaks with negligible variation with increasing salt concentration. This RDF and CN for Li-PC showed that four PC molecules surround Li in its immediate vicinity. The RDF and CN for PC-PC showed that one PC molecules in in the immediate vicinity with several more at a radial distance of 4 - 6 Å. In summary the strongest structure exists for Li-Oc atoms of PC molecules which give rise to the solvation structure and the rest of the constituent exists with each other forming a very weak structure around each other. Note that PC-PC RDF and CN with regard to the individual atoms were not shown as changing salt concentration had little to no effect on PC-PC interaction shown in Figure S10(c)(d). Similarly, weak structure can be expected for individual atoms of PC-PC interaction without noticeable change with increasing salt concentration.

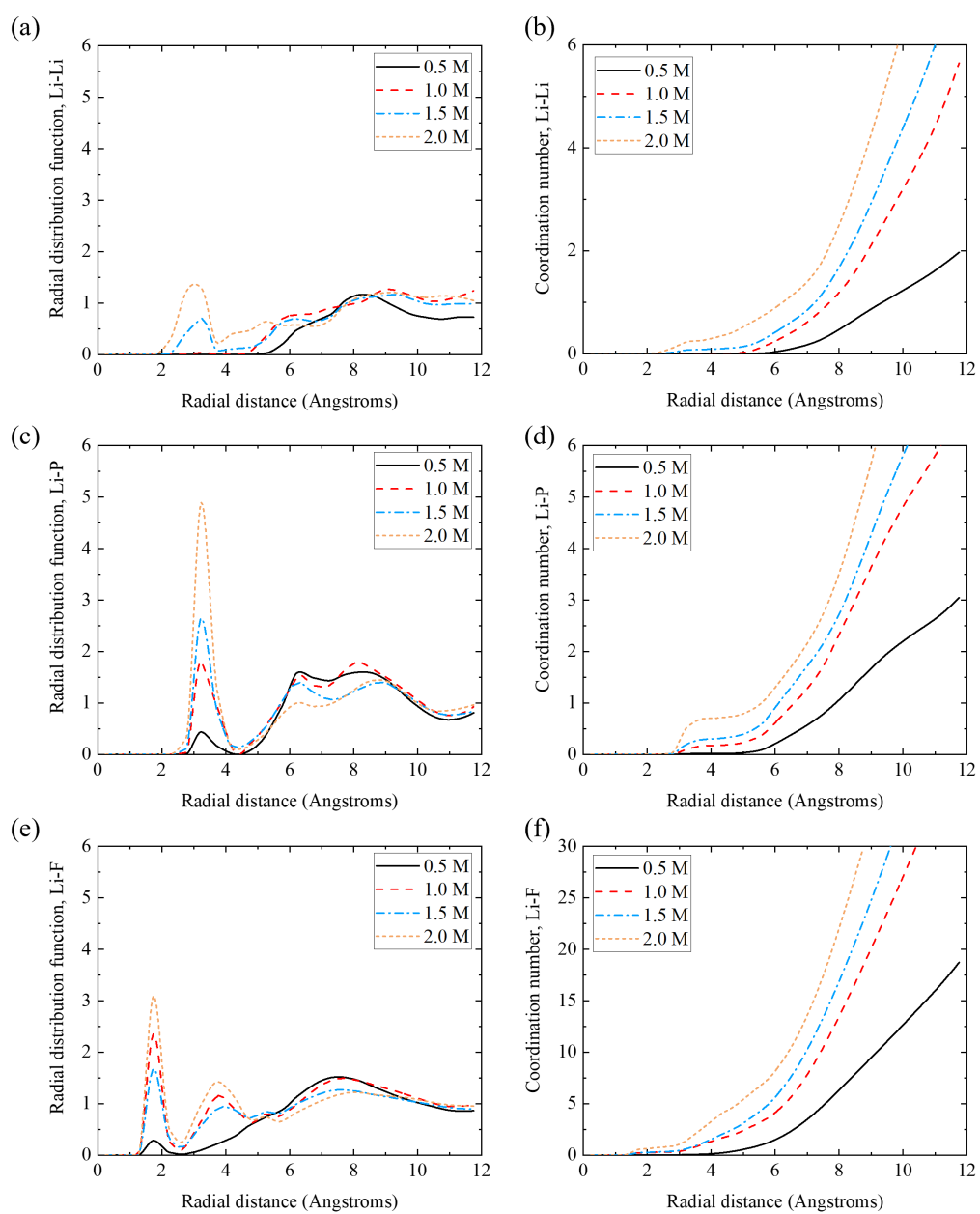


Figure S6: Radial distribution function and coordination number of (a)(b) Li-Li, (c)(d) Li-P and (e)(f) Li-F atoms in the electrolyte solution with increasing LiPF_6 concentration in PC.

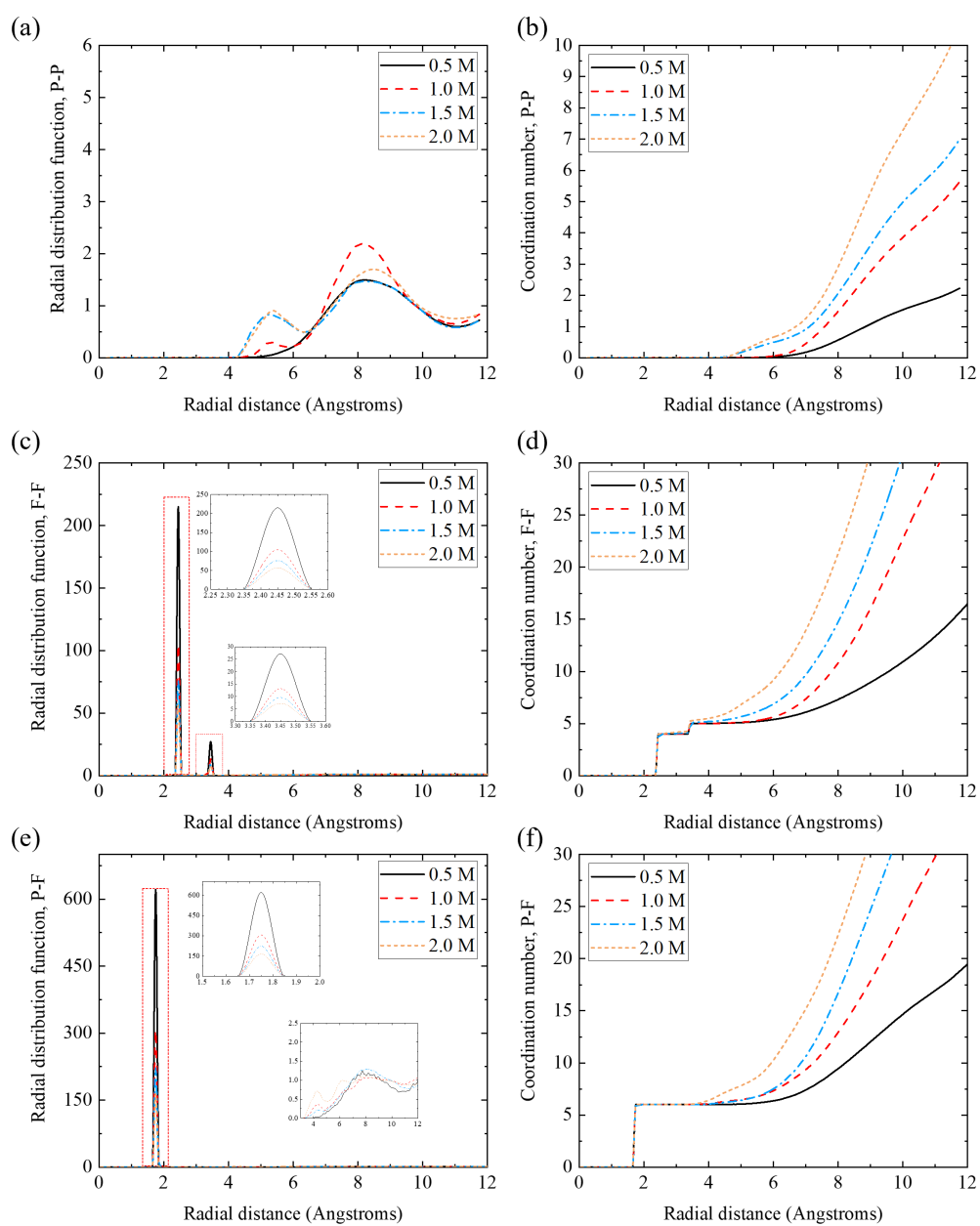


Figure S7: Radial distribution function and coordination number of (a)(b) P-P, (c)(d) F-F and (e)(f) P-F atoms in the electrolyte solution with increasing LiPF_6 concentration in PC.

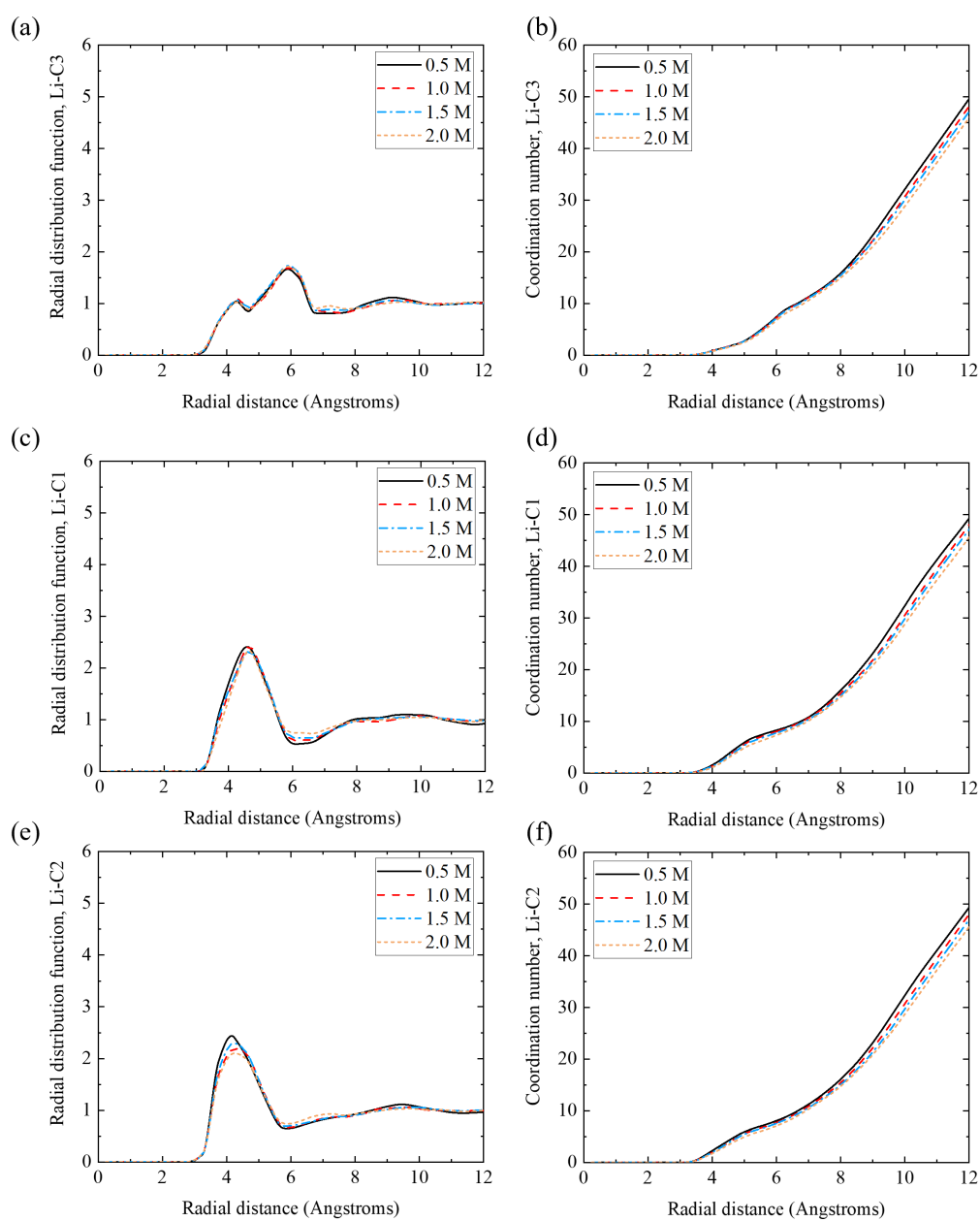


Figure S8: Radial distribution function and coordination number of (a)(b) Li-C3, (c)(d) Li-C1 and (e)(f) Li-C2 atoms in the electrolyte solution with increasing LiPF₆ concentration in PC.

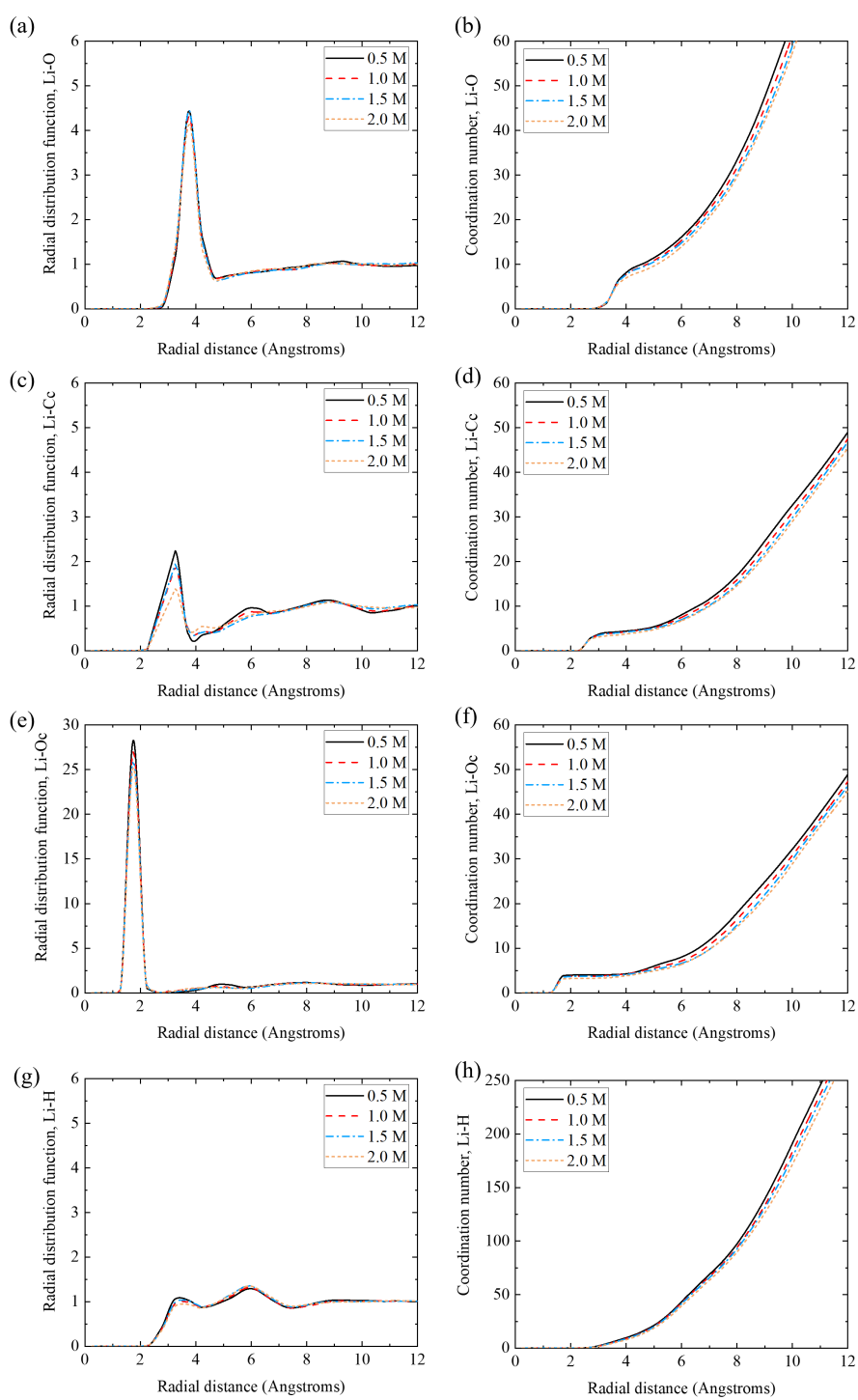


Figure S9: Radial distribution function and coordination number of (a)(b) Li-O, (c)(d) Li-Cc and (e)(f) Li-Oc (g)(h) Li-H atoms in the electrolyte solution with increasing LiPF_6 concentration in PC.

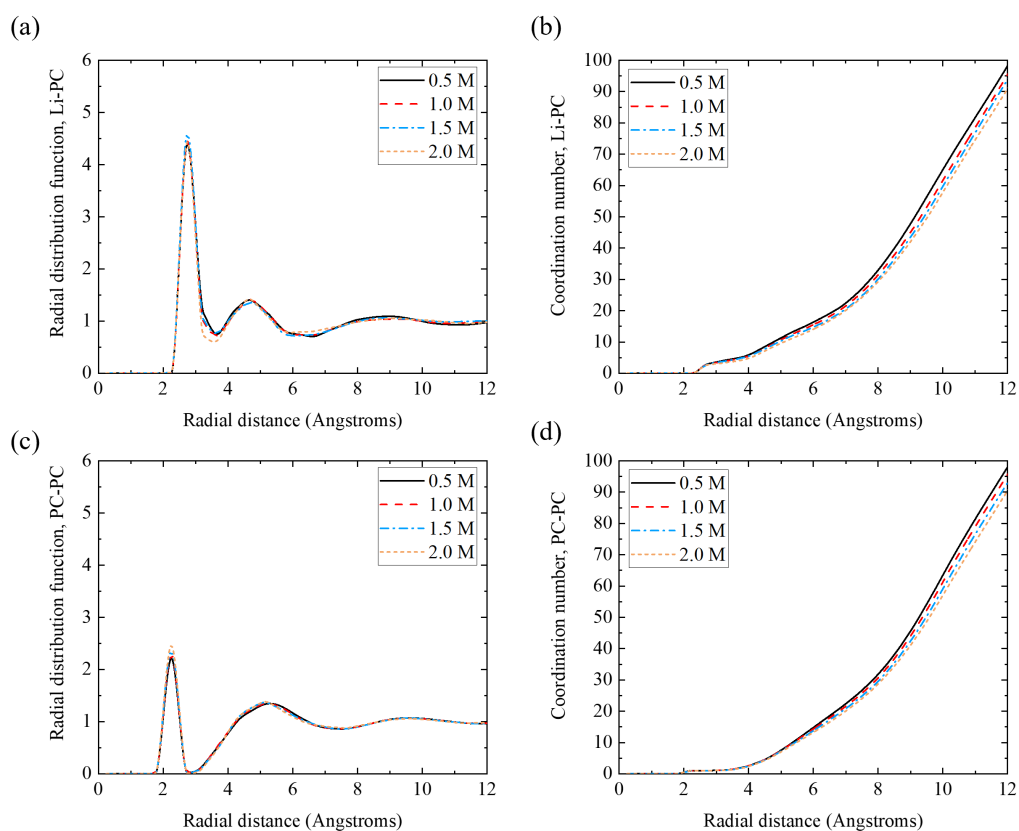


Figure S10: Radial distribution function and coordination number of (a)(b) Li-PC and (c)(d) PC-PC atoms in the electrolyte solution with increasing LiPF_6 concentration in PC.

Species charge density profiles

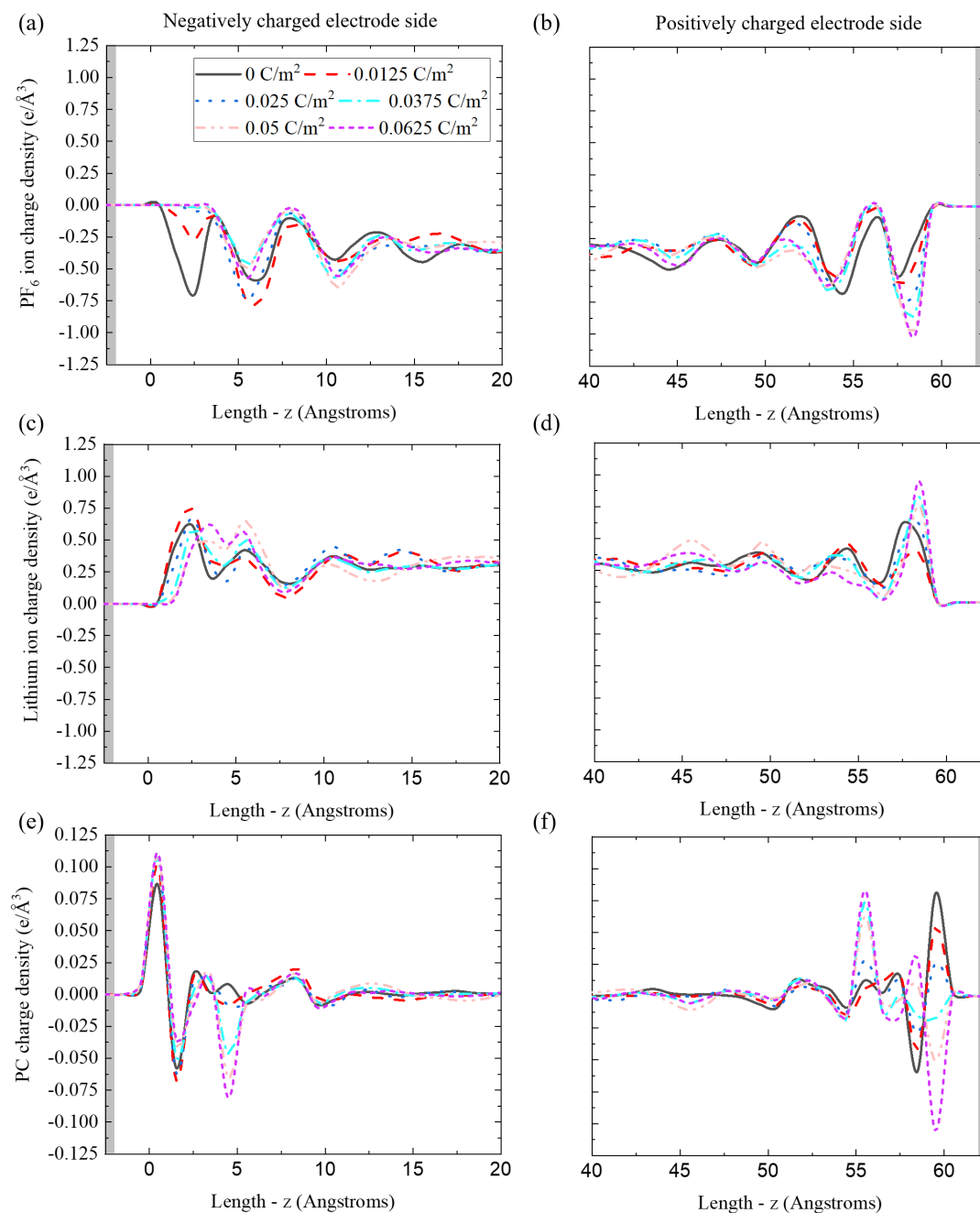


Figure S11: Charge density profile across the full domain for (a)(b) PF₆ ion, (c)(d) Li ion and (e)(f) solvent molecules for uncharged and charged electrodes.

Net charge density

Figure S12 shows the net charge density profile for the full simulation domain under both uncharged and charged electrode conditions. It shows that the net charge density fluctuated around zero charge density in the bulk indicating charge neutrality. Note that the peaks of charge density near the two uncharged and charged electrodes can be attributed to the localised ordered packing of ions induced by Van der Waals and electrostatic interactions, respectively, between the electrolyte and the electrode.

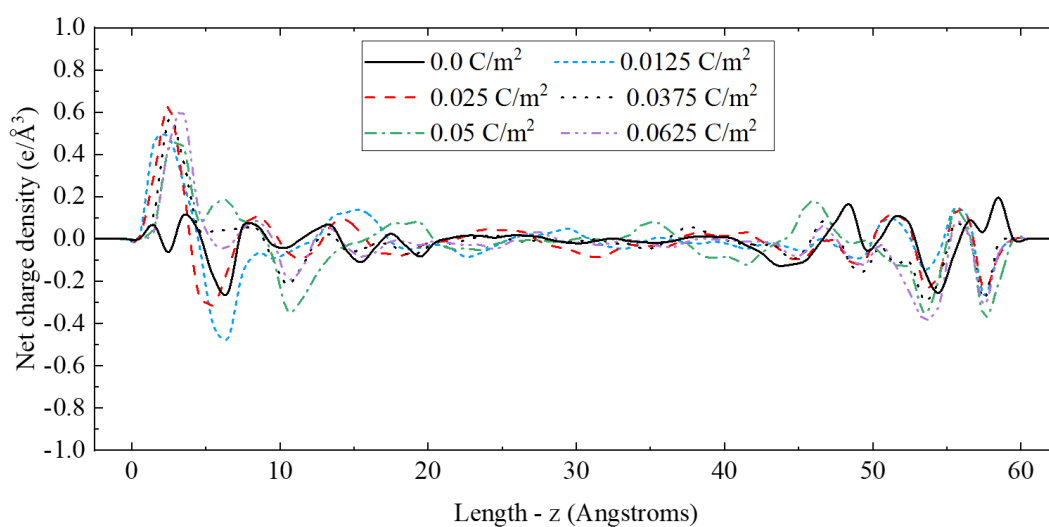


Figure S12: Net charge density profile of ionic species for uncharged (C/m^2) and charged electrode.

Species number density profiles

Figure S13 shows the number density profile across the full domain for (a)(b) PF_6^- ion, (c)(d) lithium ion and (e)(f) solvent molecules for uncharged and charged electrodes. The peaks for number density profiles near the charged electrode showed similar trend to charged density profiles with increasing surface charge density. The number density profile for solvent showed similar number density profile regardless of increasing surface charge density.

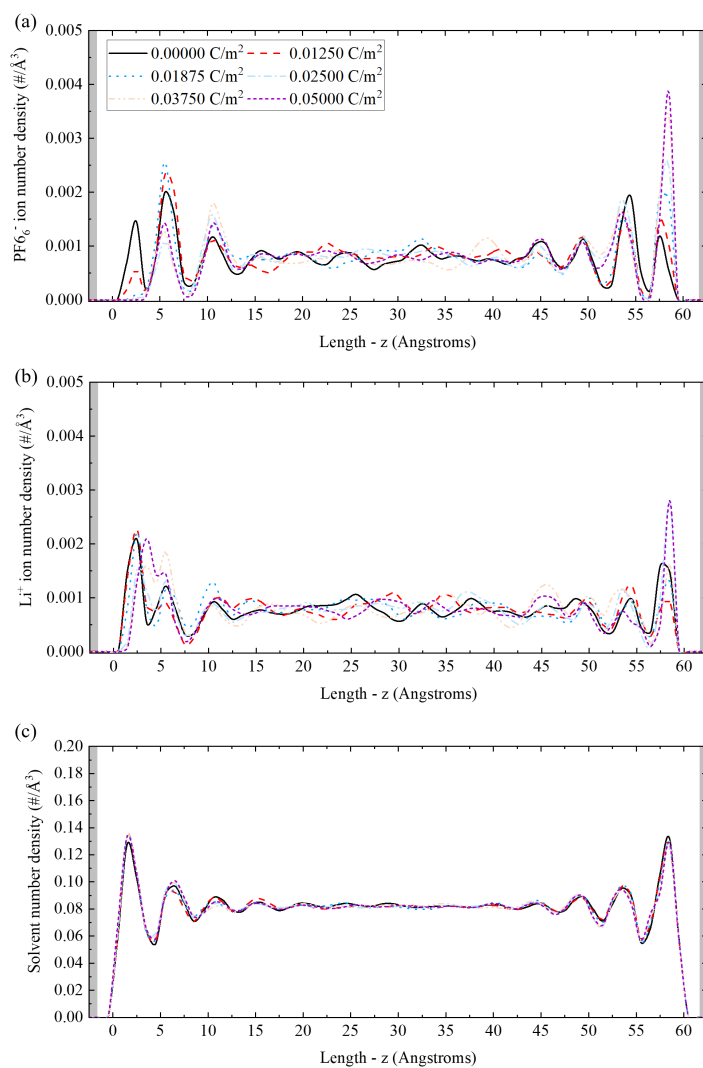


Figure S13: Number density profile across the full domain for (a)(b) PF_6^- ion, (c)(d) Li ion and (e)(f) solvent molecules for uncharged and charged electrodes.

Comparison of Species number density profiles with literature

Figure S14 shows the number density profile of ions from (a)(b) present simulation of 1M LiPF₆ in PC and (c)(d) Jorn et. al. simulation of 1M LiPF₆ in PC [11] for charged and uncharged electrodes. Note that for the present simulation the charged case corresponds to the highest surface charge density of 0.05 C/m² because Jorn et. al. only has one charged case where the net voltage induced on electrodes is 3V. The figure shows that for both present and Jorn et. al. simulation, the PF6 ions number density significantly increased near its counter electrode when the electrode was charged. The number density profile for lithium ions showed slight movement away from the counter electrode in present simulations. Meanwhile, the lithium ion showed two peaks near its counter electrode. The first peak showed no change in magnitude while the second peak showed significant rise in its magnitude when the electrode was charged. This behaviour of lithium ion near its counter electrode was unexpected. In the present simulation this unexpected behaviour was attributed to the solvation of PC with lithium ions. Similarly, the unexpected behaviour was attributed to the solvation of EC with lithium ions [11]. These qualitative similarities in number density profile and similar phenomena behind the unexpected behaviour sufficiently validate the model presented in this simulation.

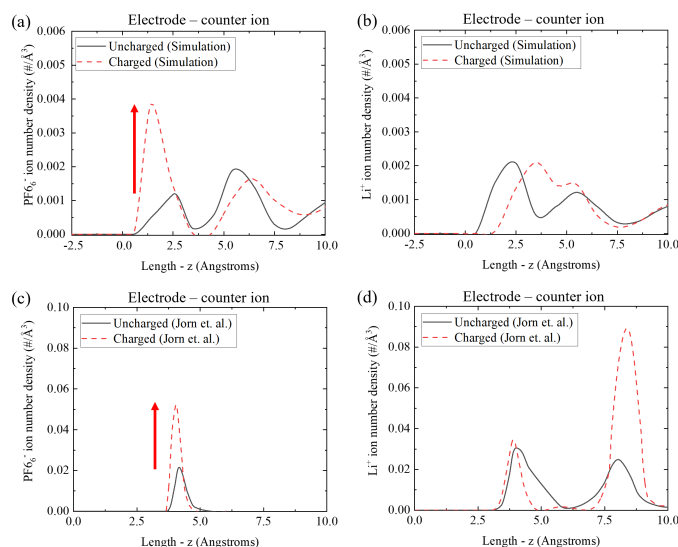


Figure S14: Number density profile of ions from (a)(b) present simulation of 1M LiPF₆ in PC and (c)(d) Jorn et. al. simulation of 1M LiPF₆ in PC [11] for charged and uncharged electrodes.

Solvation structure of hexafluorophosphate ion in PC and EC:DMC mixed solvent

Figure S15 shows (a) radial distribution and coordination number of phosphorous atom of PF_6^- ion with PC molecule along with (b) schematics. The small peak of radial distribution number compared with Li^+ ion and a coordination number of two at a 4 Å distance away from phosphorous indicated that two PC molecules could form a very weak solvation structure around the negative PF_6^- ion. This can be attributed to the weak electrostatic interaction between fluorine (-0.3450e) atoms of PF_6^- and the hydrogen (0.1325e) atoms of PC.

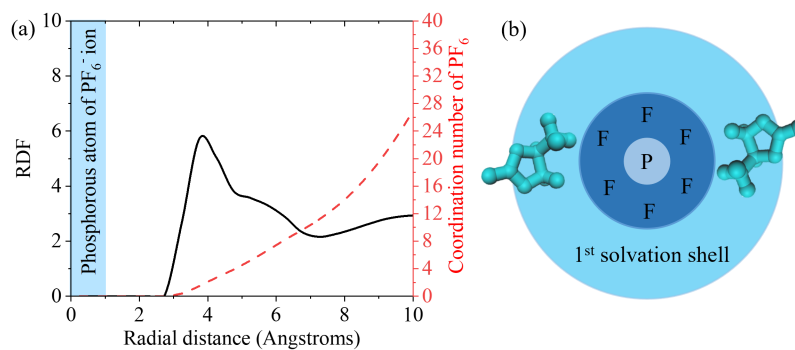


Figure S15: (a) Radial distribution function and solvation number of PF_6^- and (b) schematics of the solvation structures for PC solvent.

Residence time

Table S1 shows the residence time of solvent molecules near lithium ion for PC solvent. It indicates that the PC molecules showed a very high residence time both in the bulk electrolyte and near the electrodes during the production run time. This indicated that the PC molecule in the solvation structure were seldom substituted by other solvent molecules. This can be attributed to the strong electrostatic interaction between lithium ion and the carbonyl oxygen of PC.

Table S1: Average residence time of solvent molecules in the lithium ion solvation structure for PC

Solvent	Bulk residence time, τ_B (ns)	Negative electrode residence time, τ_N (ns)	Positive electrode residence time, τ_P (ns)
PC	80.21 ± 2.5	85.56 ± 1.9	82.37 ± 2.4

Geometric analysis of lithium solvation structure

To further calculate the distance between lithium ion and the electrode for different solvation orientation, Figure S16 shows the schematics of the tetrahedral solvation structure near negative electrode for (a) tetrahedral planner and (b) tetrahedral edge orientation of solvation structure. It shows that the distance between lithium ion and the electrode was 0.6\AA and 1.05\AA for tetrahedral planner and tetrahedral edge orientation, respectively. In other words, the change in the distance during orientation shift was 0.45\AA .

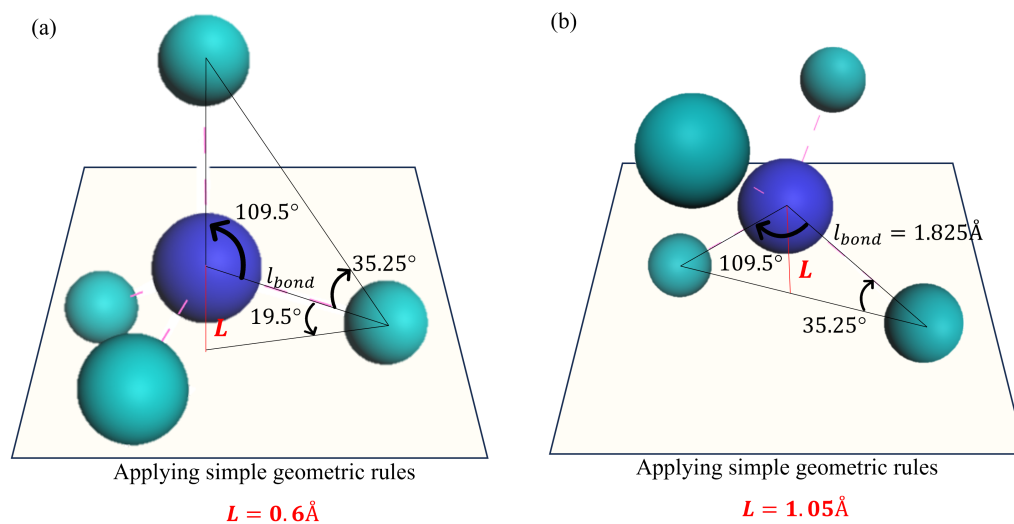


Figure S16: Geometric analysis of the distance between lithium ion and electrode with the solvation structure of (a) tetrahedral planner orientation to (b) tetrahedral edge orientation.

Snapshots of lithium ion solvation structures near charged electrodes

To begin with, Figure S17 shows the charge distribution of PC. It shows that PC have one positive and negative polar end.

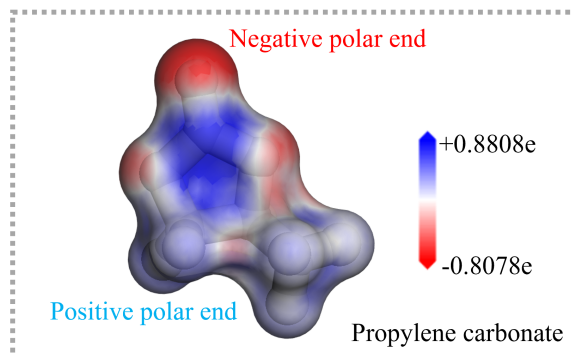


Figure S17: Charge distribution of (a) PC solvent molecules.

Figure S18 shows the snapshots of lithium ion solvation structure with PC molecules near the two electrodes at low and high surface charge density. It shows that the solvation structure had a tilted-tetrahedral planar orientation near positive and negative electrodes for pure solvent at low surface charge density. This could be attributed to the Van der Waals interaction and the absence of strong electrostatic interaction. The strong negative polar end of PC molecules in solvation structure were anchored to the positive electrode resulting in a strict tetrahedral planar orientation for high surface charge density near positive electrode. The tendency of PC molecules to vertically stand on its positive polar end shifts the orientation from tilted-tetrahedral planar orientation to tetrahedral edge orientation for high surface charge density near negative electrode. The persistence of this orientation could be attributed to the equal electrostatic attractive interaction between the polar positive end of the two PC molecules farther away from the negative electrode which balanced the solvation structure on the two standing PC molecules.

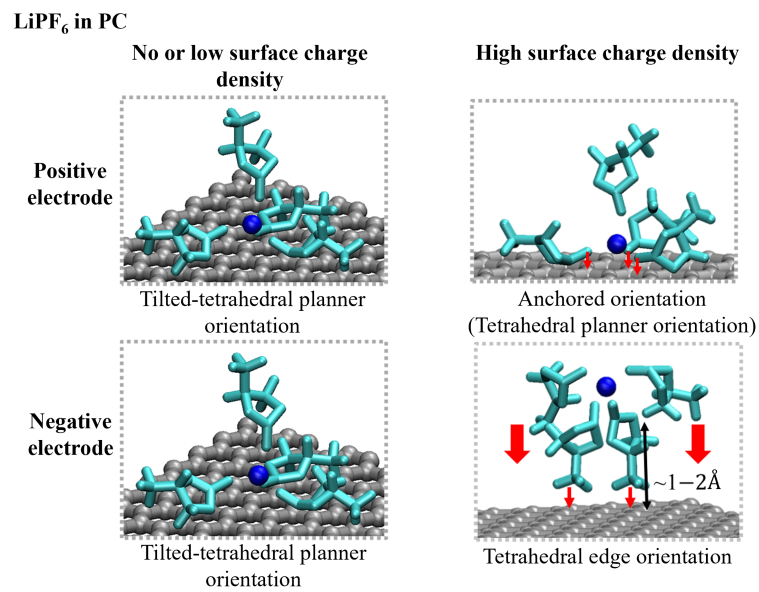


Figure S18: Snapshots of lithium ion solvation structure orientations with PC solvent molecules near the two electrodes at low and high surface charge density. Note that the red arrows shows the electrostatic attractive interaction of polar end of solvent molecules with the electrode.

References

- [1] Maple JR, Hwang MJ, Stockfisch TP, Dinur U, Waldman M, Ewig CS, et al. Derivation of class II force fields. I. Methodology and quantum force field for the alkyl functional group and alkane molecules. *Journal of Computational Chemistry*. 1994;15(2):162-82. Available from: <https://onlinelibrary.wiley.com/doi/abs/10.1002/jcc.540150207>.
- [2] Hwang MJ, Stockfisch TP, Hagler AT. Derivation of Class II Force Fields. 2. Derivation and Characterization of a Class II Force Field, CFF93, for the Alkyl Functional Group and Alkane Molecules. *Journal of the American Chemical Society*. 1994;116(6):2515-25. Available from: <https://doi.org/10.1021/ja00085a036>.
- [3] Maple JR, Hwang MJ, Stockfisch TP, Hagler AT. Derivation of Class II Force Fields. III. Characterization of a Quantum Force Field for Alkanes. *Israel Journal of Chemistry*. 1994;34(2):195-231. Available from: <https://onlinelibrary.wiley.com/doi/abs/10.1002/ijch.199400025>.
- [4] Peng Z, Ewig CS, Hwang MJ, Waldman M, Hagler AT. Derivation of Class II Force Fields. 4. van der Waals Parameters of Alkali Metal Cations and Halide Anions. *The Journal of Physical Chemistry A*. 1997;101(39):7243-52. Available from: <https://doi.org/10.1021/jp964080y>.
- [5] Maple JR, Hwang MJ, Jalkanen KJ, Stockfisch TP, Hagler AT. Derivation of class II force fields: V. Quantum force field for amides, peptides, and related compounds. *Journal of Computational Chemistry*. 1998;19(4):430-58. Available from: <https://onlinelibrary.wiley.com/doi/abs/10.1002/%28SICI%291096-987X%28199803%2919%3A4%3C430%3A%3AAID-JCC5%3E3.O.C0%3B2-T>.
- [6] Hwang MJ, Ni X, Waldman M, Ewig CS, Hagler AT. Derivation of class II force fields. VI. Carbohydrate compounds and anomeric effects. *Biopolymers*. 1998;45(6):435-68. Available from: <https://onlinelibrary.wiley.com/doi/abs/10.1002/%28SICI%291097-0282%28199805%2945%3A6%3C435%3A%3AAID-BIP3%3E3.O.C0%3B2-Q>.
- [7] Ewig CS, Thacher TS, Hagler AT. Derivation of Class II Force Fields. 7. Nonbonded Force Field Parameters for Organic Compounds. *The Journal of Physical Chemistry B*. 1999;103(33):6998-7014. Available from: <https://doi.org/10.1021/jp9910111>.
- [8] Ewig CS, Berry R, Dinur U, Hill JR, Hwang MJ, Li H, et al. Derivation of class II force fields. VIII. Derivation of a general quantum mechanical force field for organic compounds. *Journal of Computational Chemistry*. 2001;22(15):1782-800. Available from: <https://onlinelibrary.wiley.com/doi/abs/10.1002/jcc.1131>.
- [9] Avula NVS, Karmakar A, Kumar R, Balasubramanian S. Efficient Parametrization of Force Field for the Quantitative Prediction of the Physical Properties of Ionic Liquid Electrolytes. *Journal of Chemical Theory and Com-*

putation. 2021;17(7):4274-90. PMID: 34097391. Available from: <https://doi.org/10.1021/acs.jctc.1c00268>.

[10] Mynam M, Ravikumar B, Rai B. Molecular dynamics study of propylene carbonate based concentrated electrolyte solutions for lithium ion batteries. *Journal of Molecular Liquids*. 2019;278:97-104. Available from: <https://www.sciencedirect.com/science/article/pii/S0167732218348682>.

[11] Jorn R, Kumar R, Abraham DP, Voth GA. Atomistic Modeling of the Electrode–Electrolyte Interface in Li-Ion Energy Storage Systems: Electrolyte Structuring. *The Journal of Physical Chemistry C*. 2013;117(8):3747-61. Available from: <https://doi.org/10.1021/jp3102282>.